VSP

Advanced Composite Materials 18 (2009) 251–264

ADVANCED COMPOSITE MATERIALS
www.brill.nl/acm

Characterization of Nonlinear Behaviors of CSCNT/Carbon Fiber-Reinforced Epoxy Laminates

Tomohiro Yokozeki [a,*], **Yutaka Iwahori** [b], **Masaru Ishibashi** [c] **and Takashi Yanagisawa** [c]

[a] Department of Aeronautics and Astronautics, The University of Tokyo, 7-3-1 Hongo, Bunkyo-ku, Tokyo 113-8656, Japan

[b] Advanced Materials Group, Aerospace Research and Development Directorate, Japan Aerospace Exploration Agency, 6-13-1 Osawa, Mitaka, Tokyo 181-0015, Japan

[c] GSI Creos Corporation 1-12, Minami-Watarida, Kawasaki-ku, Kawasaki, Kanagawa 210-0855, Japan

Received 19 March 2007; accepted 8 August 2008

Abstract

Nonlinear mechanical behaviors of unidirectional carbon fiber-reinforced plastic (CFRP) laminates using cup-stacked carbon nanotubes (CSCNTs) dispersed epoxy are evaluated and compared with those of CFRP laminates without CSCNTs. Off-axis compression tests are performed to obtain the stress–strain relations. One-parameter plasticity model is applied to characterize the nonlinear response of unidirectional laminates, and nonlinear behaviors of laminates with and without CSCNTs are compared. Clear improvement in stiffness of off-axis specimens by using CSCNTs is demonstrated, which is considered to contribute the enhancement of the longitudinal compressive strength of unidirectional laminates and compressive strength of multidirectional laminates. Finally, longitudinal compressive strengths are predicted based on a kink band model including the nonlinear responses in order to demonstrate the improvement in longitudinal strength of CFRP by dispersing CSCNTs.

Keywords

Polymer–matrix composites, nonlinear behaviors, compressive strength, cup-stacked carbon nanotube

1. Introduction

Extensive attention has been paid to nano-fillers as the superior candidate for high-performance reinforcements of engineering polymers. Many types of nanofibers and nanoparticles (e.g., carbon nanotubes, CNTs) have been incorporated into the traditional polymers in order to enhance the mechanical properties as well as to add

* To whom correspondence should be addressed. E-mail: yokozeki@aastr.t.u-tokyo.ac.jp
Edited by JSCM

 DOI:10.1163/156855109X428781

multifunctionality (e.g., thermal, electrical and gas/liquid barrier properties) [1–6]. Moderate increase in stiffness of polymers by using nano-fillers has been widely reported [7–10].

Increase in stiffness of polymers is considered to result in mechanical benefits for fiber-reinforced composite laminates. One of the most promising advantages is an increase in compressive strength of unidirectional laminates in the fiber direction. As is indicated in the classical fiber microbuckling analysis [11, 12], longitudinal compressive strength of unidirectional laminates is proportional to shear modulus of matrix or composites. Subramaniyan and Sun [13] demonstrated the enhancement of compressive strength of glass fiber-reinforced plastic (GFRP) unidirectional laminates using nanoclays. They evaluated nonlinear behaviors of resin and compressive strength of off-axis (5, 10 and 15°) unidirectional specimens, which were cured using a vacuum assisted wet layup process. The predicted strengths using elastic–plastic model confirm the enhancement in compressive strength by addition of nanoclay.

Cup-stacked carbon nanotube (CSCNT) is also considered to be a superior candidate as a polymer modifier [14]. Figure 1(a) shows the schematic view of the CSCNT, CARBERE®, manufactured by GSI Creos Corporation. This type of CNT has novel structural characteristics such as a larger hollow core and a larger portion of open ends than other CNTs. Several layers of truncated conical graphene sheets are stacked and placed in relation to each other like metal bellows. The stacking morphology of the truncated conical graphene sheets exhibits an angle to the fiber axis, and almost every portion of the graphene sheet edges are exposed to the outside. This nano-structure of CSCNT suggests the advantage in the load transfer between CSCNT and polymer matrix to prevent graphene sheet sliding. Because there are no C–C bonds between any two adjacent graphene sheet cups, CSCNTs have much lower mechanical properties than single-walled/multi-walled CNTs. Nevertheless, they are expected to exhibit excellent mechanical properties compared to the conventional carbon fibers [15]. Therefore, dispersion of CSCNTs into the polymers results in the improvement of the mechanical and electric properties of the polymers [15, 16].

Mechanical properties of CFRP laminates can be also improved by using CSCNT-dispersed epoxy as indicated in the results by Iwahori *et al.* [15] and Yokozeki *et al.* [17, 18]. Although compressive strength increase of unidirectional laminates has not been confirmed because unwanted failures (e.g., splitting, brooming failures) occur during the usual compressive tests, it was demonstrated that compressive strength of quasi-isotropic laminates with CSCNTs was higher than that of laminates without CSCNTs [15, 18]. As described in this section, enhancement of shear instability of matrix or composites is considered to be the main reason for this improvement in compressive strength.

The main goal of this research is to characterize the nonlinear behaviors of unidirectional CFRP using epoxy with and without CSCNTs. Compression tests of off-axis unidirectional specimens are performed, and nonlinear stress–strain rela-

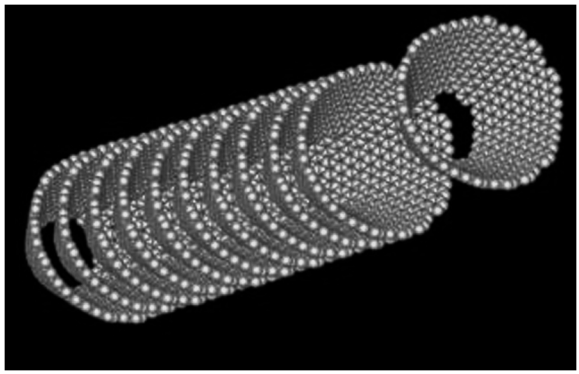

(a)

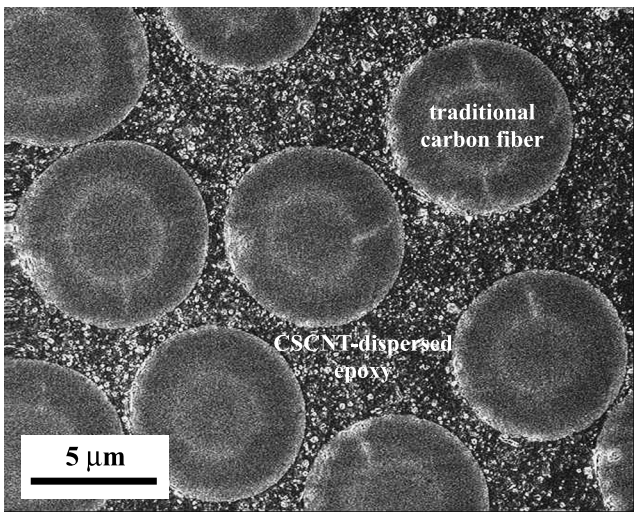

(b)

Figure 1. Schematic view of CARBERE® and cross-sectional view of 5 wt%-laminate. (a) Schematic view of CARBERE®. (b) Cross-sectional view of fabricated 5 wt%-laminates.

tions are obtained. A simple elastic–plastic constitutive model for unidirectional composites by Sun and Chen [19] is applied to the present test results. Finally, predicted results of compressive strength are presented using the obtained characterization results and a kink band model [20], and improvement in compressive strength of unidirectional laminates resulting from addition of CSCNT is semi-empirically demonstrated.

2. Experiment

2.1. Material

The CSCNTs used in this study were CARBERE® (GSI Creos Corporation), synthesized by chemical vapor deposition (CVD) using a floating reactant method [14].

For successful dispersion of CSCNTs into the polymer, CSCNTs were subjected to the dry mill using ceramic beads to control the lengths of CSCNTs. In this study, the nominal aspect ratio of CSCNTs was set to be 10 and no surface functionalization was applied to the CSCNTs. The resins used were bisphenol-A based epoxy, EP827 (Japan Epoxy Resin Co. Ltd), and dicyandiamide was used as the curing agent. The detailed dispersion procedure of CSCNTs is given in [17, 18].

Unidirectional prepregs were developed using T700SC-12K fibers and CSCNT-dispersed epoxy (0 wt% and 5 wt%) by GSI Creos Corporation, which are now commercially available. The prepreg fiber areal weight was set to 125 g/m^2 and the nominal resin content including CSCNTs was 35 wt%. Unidirectional $[0]_{36}$ laminates were stacked and fabricated using an autoclave. The stacked prepregs were subjected to a pressure of 490 kPa and to a curing temperature of 130°C for the duration of two hours. The resulting volume fractions of the carbon fiber were 60%. In this study, CFRP laminates using epoxy with 0 wt% and 5 wt% CSCNTs are referred to as 0 wt%-laminates and 5 wt%-laminates, respectively. The cross-sectional view of the fabricated 5 wt%-CFRP is shown in Fig. 1(b). Well-dispersed CSCNTs can be recognized in the matrix regions.

2.2. Experimental Procedure

Off-axis specimens with 80 mm length and 10 mm width were prepared by cutting the specimens of 0 wt%-laminates and 5 wt%-laminates with off-axis angles of 15°, 30°, 45°, 60°, and 90° (two specimens for each angle). Oblique end tabs were adopted for off-axis specimens in reference to Sun and Chung [21] to measure accurate nonlinear stress–strain curves using small specimens. Kawai *et al.* [22] demonstrated that oblique tabs are effective in order to obtain accurate stress–strain relations during off-axis tension tests even in the case of aspect ratio in the gauge section (length/width) of 4. Therefore, the aspect ratio was set to 4 in this study. The oblique end tabs were bonded to the specimens using epoxy adhesives at the oblique angles to the loading axis. The specimen configuration is shown in Fig. 2. The oblique angles were calculated in accordance with [21] using mate-

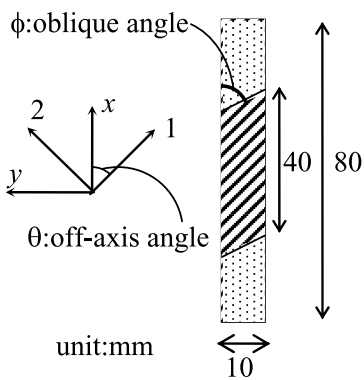

Figure 2. Specimen configuration used for off-axis compression tests.

rial properties obtained in the previous study [17], and summarized in Table 1. Because the calculated oblique angles of 0 wt%- and 5 wt%-laminates are almost same for all off-axis angles, the oblique angles shown in Table 1 were used for both laminates. Note that the selected configuration is not suitable for the evaluation of compressive strengths because the gauge length of the specimen is long compared to the thickness (about 4 mm), which results in buckling failures of specimens. However, accurate measurement of stress–strain relations of off-axis specimens including nonlinear responses is the major concern in this experiment. Therefore, the above-described specimen configuration was used in this study.

Back-to-back strain gauges were attached to specimens in longitudinal and transverse directions. Compression tests of off-axis specimens were carried out using an originally developed testing device consisting of clamping steel plates and a supporting (against the global buckling) plate (see Fig. 3). Compression loading was applied to the specimens using a mechanical-driven testing machine (4482, Instron Co. Ltd.) at a crosshead speed of 0.5 mm/min at room temperature (25°C).

Table 1.
Oblique tab angles of off-axis specimens

Off-axis angle θ (°)	15	30	45	60	90
Oblique angle φ (°)	24	38	57	75	90

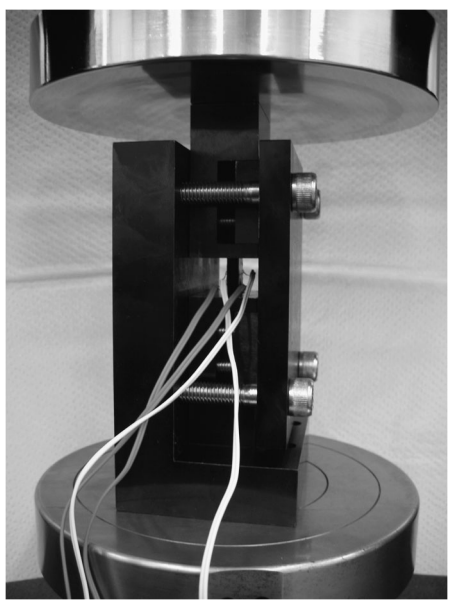

Figure 3. Apparatus of off-axis compression test.

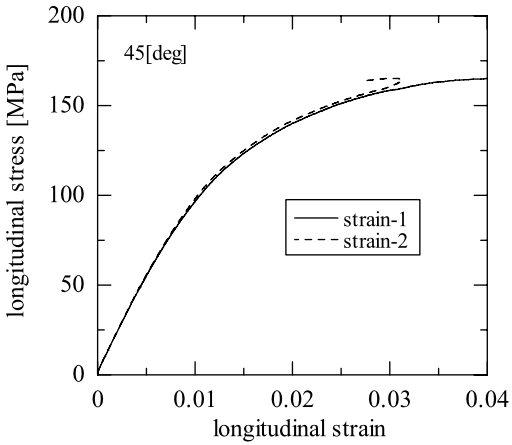

Figure 4. Stress–strain relations obtained from back-to-back strain gauges.

2.3. Experimental Results

As mentioned in Section 2.2, the specimen configuration is relatively long, and thus, specimens except 15° laminates failed due to buckling. A typical example of the measured stress–strain relation (45° specimen) using back-to-back strain gauges is shown in Fig. 4, which exhibits clear strain reversal before failure. Thus, nonlinear stress–strain relations were determined from the averaged strains of back-to-back gauges using the data prior to such a strain reversal.

The obtained stress–strain curves of 0 wt%-laminates and 5 wt%-laminates are compared in Fig. 5. Although two specimens were used in the present experiment for each off-axis angle, stress–strain curves exhibit almost identical behaviors among the specimens with same configuration. In addition, 0 wt%-laminates and 5 wt%-laminates show clearly different stress–strain curves. Elastic Young's moduli and elastic Poisson's ratios of the off-axis specimens were evaluated from these curves, the data corresponding to the longitudinal strains of 0.1–0.3%. Plastic Poisson's ratios, which were almost constant values at any stress level within this study, were also evaluated under the assumption that elastic strains are linear. These properties are summarized in Table 2 and the obtained elastic constants are summarized in Table 3. In-plane shear modulus (G_{LT}) was determined using 45° off-axis data and the following equation,

$$G_{LT} = \frac{E_{45}}{2(1 + \nu_{45})}, \tag{1}$$

where E_{45} and ν_{45} are Young's modulus and Poisson's ratio of 45° off-axis specimens, respectively. Note that average values obtained from two specimens for each angle are listed in Table 2, and the obtained elastic constants exhibited relatively small scatter between the two specimens. It can be concluded that 5 wt%-laminates are stiffer than 0 wt%-laminates for all off-axis specimens, and transverse Young's

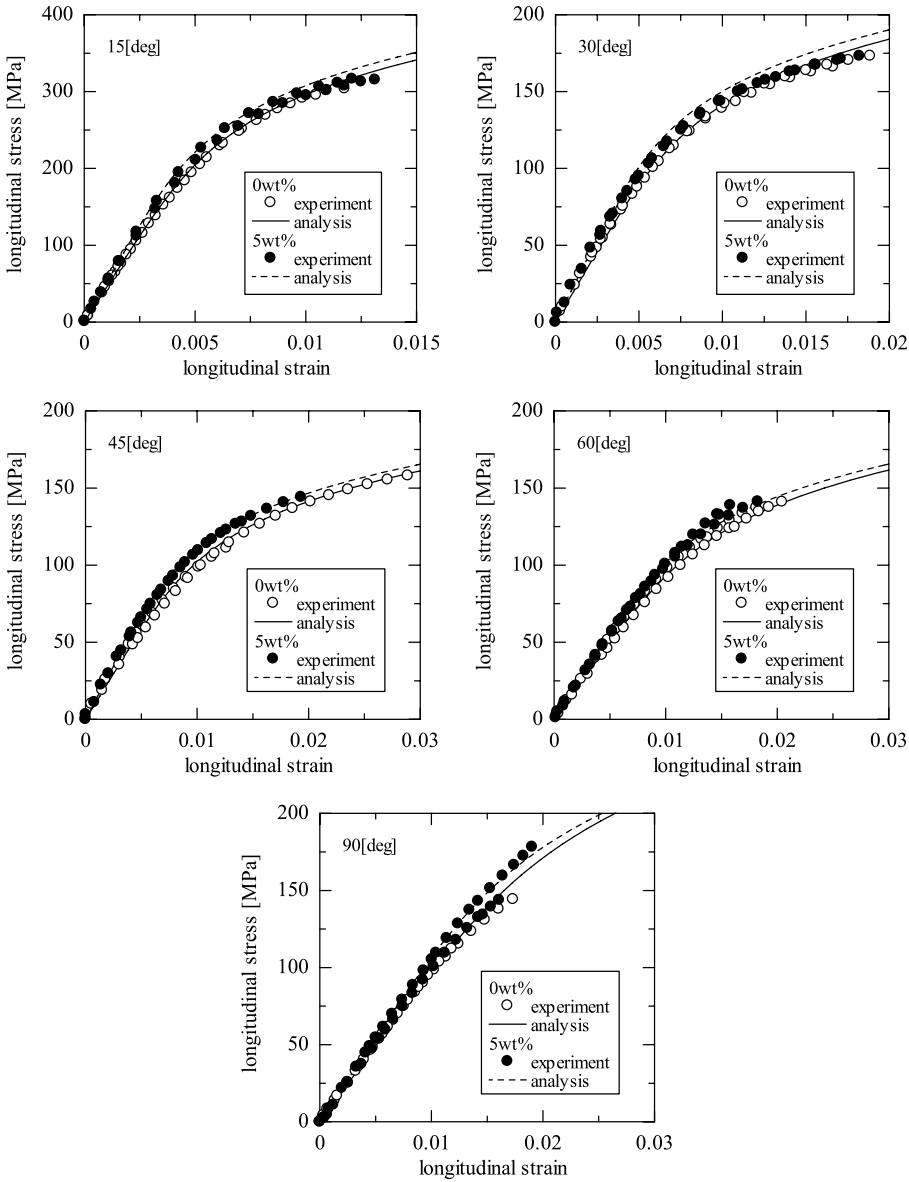

Figure 5. Comparison of stress–strain curves between 0 wt%- and 5 wt%-laminates.

modulus and in-plane shear stiffness increase due to addition of CSCNTs into CFRP laminates.

3. Elastic–Plastic Modeling

This section describes a characterization method for the elastic–plastic behaviors of off-axis specimens. In this study, mechanical properties of 'homogeneous' unidirec-

Table 2.
Measured Young's moduli, elastic Poisson's ratios and plastic Poisson's ratios

	Off-axis angle (°)	Young's modulus E_x (GPa)	Elastic Poisson's ratio ν^{e}	Plastic Poisson's ratio ν^{p}
0 wt%	15	41.4	0.46	1.21
	30	18.1	0.42	0.94
	45	12.0	0.35	0.75
	60	10.1	0.20	0.50
	90	9.8	0.02	0.04
5 wt%	15	46.2	0.43	1.14
	30	19.8	0.38	0.92
	45	13.2	0.31	0.78
	60	11.5	0.19	0.51
	90	10.9	0.03	0.01

Table 3.
Summary of material parameters

	0 wt%	5 wt%
E_{L} (GPa)	117*	117*
E_{T} (GPa)	9.8	10.9
ν_{LT}	0.32*	0.32*
G_{LT} (GPa)	4.3	5.1
a_{66}	3.4	3.2
A (MPa^{-n})	4.54×10^{-16}	4.85×10^{-16}
n	5.46	5.47

* Assumed values with consideration of results in [17].

tional composites are utilized instead of treating the fiber and matrix separately. Unidirectional CFRP composites exhibit linear elasticity in the fiber direction, whereas other properties (e.g., shear properties) are assumed to exhibit elastic–plastic behaviors. To characterize the elastic–plastic properties of unidirectional composites precisely but simply, we apply Sun and Chen's one-parameter plasticity model [19] to the constitutive behaviors of unidirectional composites.

It is assumed that total strain can be decomposed into elastic and plastic strains within infinitesimal strain conditions, as

$$\mathrm{d}\varepsilon_{ij} = \mathrm{d}\varepsilon_{ij}^{\mathrm{e}} + \mathrm{d}\varepsilon_{ij}^{\mathrm{p}}, \tag{2}$$

where superscripts e and p respectively denote elastic and plastic, and 'elastic' means linear elastic in this study. The incremental form of the elastic constitutive

equation under a plane stress state is expressed as

$$\begin{Bmatrix} \mathrm{d}\varepsilon_{11}^{\mathrm{e}} \\ \mathrm{d}\varepsilon_{22}^{\mathrm{e}} \\ \mathrm{d}\gamma_{12}^{\mathrm{e}} \end{Bmatrix} = \begin{bmatrix} 1/E_{\mathrm{L}} & -\nu_{\mathrm{LT}}/E_{\mathrm{L}} & 0 \\ & 1/E_{\mathrm{T}} & 0 \\ \mathit{sym} & & 1/G_{\mathrm{LT}} \end{bmatrix} \begin{Bmatrix} \mathrm{d}\sigma_{11} \\ \mathrm{d}\sigma_{22} \\ \mathrm{d}\tau_{12} \end{Bmatrix}. \tag{3}$$

Note that the 1 and 2-directions are defined respectively as the fiber (L) and in-plane transverse (T) to the fiber direction. To model the plastic constitutive relation, Sun and Chen [19] defined the effective stress under plane stress condition as

$$\bar{\sigma} = \sqrt{\frac{3}{2}\left(\sigma_{22}^2 + 2a_{66}\tau_{12}^2\right)}, \tag{4}$$

where a_{66} is an anisotropic parameter. In addition, the effective stress–strain relation is approximated by the power law:

$$\bar{\varepsilon}^{\mathrm{p}} = A\bar{\sigma}^n. \tag{5}$$

Thus, the following incremental plastic constitutive relation is obtained [23]:

$$\begin{Bmatrix} \mathrm{d}\varepsilon_{11}^{\mathrm{p}} \\ \mathrm{d}\varepsilon_{22}^{\mathrm{p}} \\ \mathrm{d}\gamma_{12}^{\mathrm{p}} \end{Bmatrix} = \frac{9}{4}nA\bar{\sigma}^{n-3} \begin{bmatrix} 0 & 0 & 0 \\ 0 & \sigma_{22}^2 & 2a_{66}\sigma_{22}\tau_{12} \\ 0 & 2a_{66}\sigma_{22}\tau_{12} & 4a_{66}^2\tau_{12}^2 \end{bmatrix} \begin{Bmatrix} \mathrm{d}\sigma_{11} \\ \mathrm{d}\sigma_{22} \\ \mathrm{d}\tau_{12} \end{Bmatrix}. \tag{6}$$

This elastic–plastic model can be easily applied to off-axis tests [19]. Let the $(x-y)$ coordinate and the (1–2) coordinate respectively represent the global and the local (material principal) axes (see Fig. 2). Under uniaxial loading, the stresses in the local coordinate are expressed as

$$\begin{aligned} \sigma_{11} &= \sigma_x \cos^2\theta, \\ \sigma_{22} &= \sigma_x \sin^2\theta, \\ \tau_{12} &= -\sigma_x \sin\theta\cos\theta, \end{aligned} \tag{7}$$

where θ is an off-axis angle. The effective stress and effective plastic strain under uniaxial loading are

$$\begin{aligned} \bar{\sigma} &= h(\theta)\sigma_x, \\ \bar{\varepsilon}^{\mathrm{p}} &= \frac{\varepsilon_x^{\mathrm{p}}}{h(\theta)}, \end{aligned} \tag{8}$$

where

$$h(\theta) = \begin{cases} \sqrt{\frac{3}{2}\sin^4\theta + 3a_{66}\sin^2\theta\cos^2\theta}, & \sigma_x \geqslant 0, \\ -\sqrt{\frac{3}{2}\sin^4\theta + 3a_{66}\sin^2\theta\cos^2\theta}, & \sigma_x \leqslant 0. \end{cases} \tag{9}$$

Therefore, the effective stress and effective plastic strain can be expressed simply in terms of experimental values in off-axis tests. Experimental results of off-axis

compression tests are convertible to effective stress-effective plastic strain relation using (5), (8) and

$$\varepsilon_x^{\mathrm{p}} = \varepsilon_x - \frac{\sigma_x}{E_x}. \tag{10}$$

The effective stress-effective plastic strain relation depends on the choice of a_{66}. The values of this parameter should be selected so that all curves derived from different off-axis specimens collapse into a single curve.

The plastic Poisson's ratios of off-axis specimens can be predicted based on a one-parameter plasticity model using the following equation [19]:

$$\nu_\theta^{\mathrm{p}} = -\frac{\mathrm{d}\varepsilon_y^{\mathrm{p}}}{\mathrm{d}\varepsilon_x^{\mathrm{p}}} = \frac{2a_{66} - 1}{2a_{66} + \tan^2\theta}. \tag{11}$$

4. Discussions

4.1. Characterization of Nonlinear Behaviors

The effective stress-effective plastic strain relations for 0 wt%- and 5 wt%-laminates based on off-axis tests are shown in Fig. 6. The obtained parameters are summarized in Table 3. The analytical stress–strain curves using the obtained parameters are compared with experimental results as shown in Fig. 5. Good correlation between experimental and analytical curves is observed for all off-axis compression tests. The predicted in-plane plastic Poisson's ratios are plotted in Fig. 7, which shows a comparison to experimental results. Although Fig. 7 indicates a slight disparity between the predictions and the experimental results, specifically in the cases of low off-axis angles, it is demonstrated that nonlinear behaviors in unidirectional 0 wt%- and 5 wt%-laminates can be successfully characterized using the one-parameter model.

It is noteworthy that the obtained power law parameters (A and n) of the effective stress-effective plastic relations are almost identical between 0 wt%- and 5 wt% laminates. However, the plastic anisotropic parameter (a_{66}) of 5 wt%-laminates is slightly lower than 0 wt%-laminates. Therefore, addition of CSCNTs into epoxy matrix is considered to induce not only increase in off-axis stiffnesses as described in Section 2.3 but also decrease in the plastic anisotropic parameters. The decrease in the parameter a_{66} corresponds to the decrease in contribution of shear stress to plastic behaviors (see (4)). These results indicate that CSCNT-dispersed CFRP laminates have more resistance against shear instability than CFRP laminates without CSCNTs, and thus, the former is expected to have higher compressive strength in the fiber direction. The following section describes some discussions on longitudinal compressive strength.

4.2. Longitudinal Compressive Strength

Many researchers indicated that shear response of resin or unidirectional composites controls the compressive strength of longitudinal compressive strength of

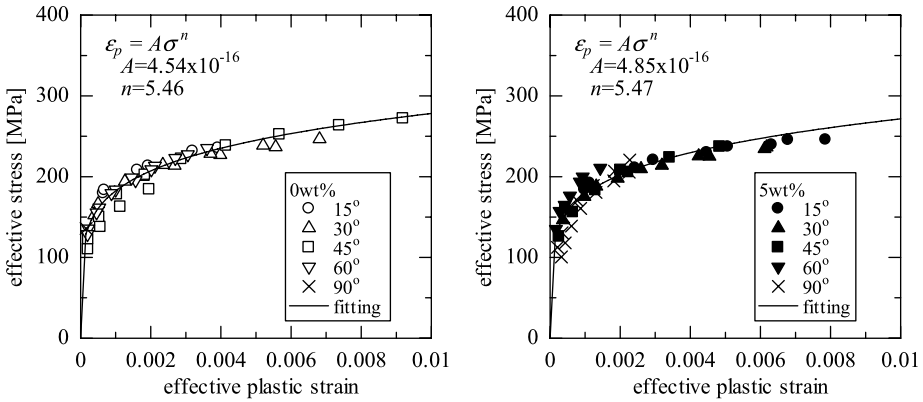

Figure 6. Effective stress-effective plastic strain curves; (left) 0 wt%-laminates, (right) 5 wt%-laminates.

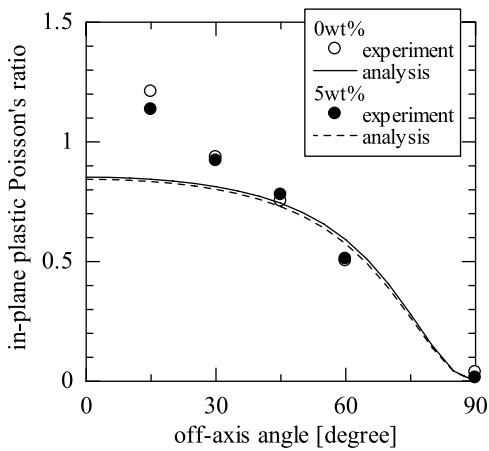

Figure 7. Comparison of measured and predicted plastic Poisson's ratios.

unidirectional laminates [24–26] using microbuckling models or kink band models. Therefore, the in-plane shear stress-shear strain relation is calculated using the parameters obtained in this study. Using (3), (4) and (6) with integration, pure shear response of unidirectional laminates can be expressed as

$$\gamma_{12} = \frac{\tau_{12}}{G_{\mathrm{LT}}} + A(\sqrt{3a_{66}})^{n+1}\tau_{12}^{n}. \tag{12}$$

The predicted pure shear stress–strain responses of 0 wt%- and 5 wt%-laminates are compared in Fig. 8. The 5 wt%-laminates exhibit stiffer shear response than 0 wt%-laminates, and thus, the former is expected to have higher longitudinal compressive strength.

Actually, longitudinal compressive strengths are predicted using a kink band model [20] combined with the constitutive relations as shown in (3) and (6). It

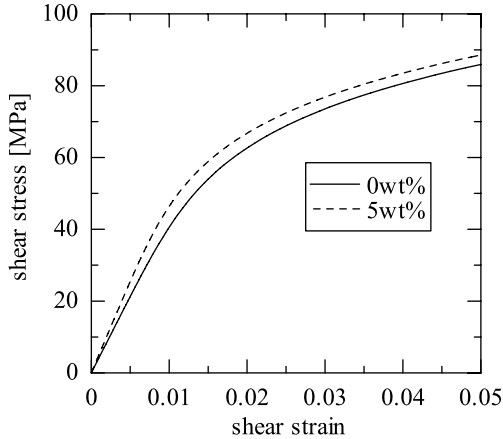

Figure 8. Comparison of pure shear stress–shear strain relations (prediction).

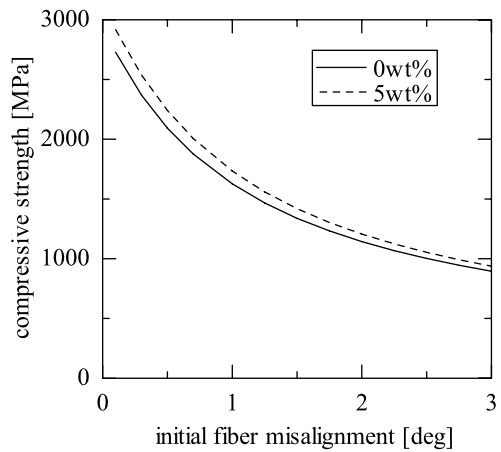

Figure 9. Comparison of predicted compressive strength.

is well-known that the predicted compressive strengths highly depend on the assumed initial fiber misalignment. Therefore, the predicted compressive strengths are plotted in Fig. 9 as a function of initial fiber misalignment. The predicted results indicate that the 5 wt%-laminates have slight higher (5–7%) compressive strengths than 0 wt%-laminates. It is semi-empirically demonstrated that CSCNT addition results in the improvement in longitudinal compressive strength of unidirectional laminates. This result supports the experimental results of compressive strength improvement of quasi-isotropic laminates [18].

Ideally, increase in amount of CSCNT dispersion would result in increase in compressive strength, whereas quality of the fabricated composites may decrease when the volume of CSCNT increases. It is interesting to study the optimal CSCNT volume for the improvement of matrix-dominated properties of laminates (e.g., compressive strength).

5. Conclusions

In this study, nonlinear mechanical behaviors of unidirectional CFRP laminates using CSCNT-dispersed epoxy were evaluated and compared with those of CFRP laminates without CSCNTs. Off-axis compression tests were performed to obtain the stress–strain relations. A one-parameter plasticity model was applied to characterize the nonlinear response of unidirectional laminates. Addition of CSCNTs into epoxy matrix resulted in not only increase in off-axis stiffnesses but also decrease in the plastic anisotropic parameters, which corresponds to increase in resistance against shear instability of unidirectional laminates. Finally, longitudinal compressive strength of unidirectional laminates was predicted using a kink band model. It was semi-empirically demonstrated that CSCNT addition results in the improvement in longitudinal compressive strength of unidirectional CFRP.

References

1. L. S. Schadler, Polymer-based and polymer-filled nanocomposites, in: *Nanocomposite Science and Technology*, P. M. Ajayan, L. S. Schadler and P. V. Braun (Eds), pp. 77–153. Wiley-VCH, Weinheim, Germany (2003).
2. W. Liu, S. V. Hoa and M. Pugh, Fracture toughness and water uptake of high-performance epoxy/nanoclay nanocomposites, *Compos. Sci. Technol.* **65**, 2364–2373 (2005).
3. D. M. Delozier, K. A. Watson, J. G. Smith and J. W. Connell, Preparation and characterization of space durable polymer nanocomposite films, *Compos. Sci. Technol.* **65**, 749–755 (2005).
4. J. K. Kim, C. Hu, R. S. C. Woo and M.-L. Sham, Moisture barrier characteristics of organoclay-epoxy nanocomposites, *Compos. Sci. Technol.* **65**, 805–813 (2005).
5. B.-K. Zhu, S.-H. Xie, Z.-K. Xu and Y.-Y. Xu, Preparation and properties of polyimide/multi-walled carbon nanotubes (MWCTs) nanocomposites, *Compos. Sci. Technol.* **66**, 548–554 (2006).
6. T. Ogasawara, Y. Ishida, T. Ishikawa, T. Aoki and T. Ogura, Helium gas permeability of montmorillonite/epoxy nanocomposites, *Composites Part A* **37**, 2236–2240 (2006).
7. E. T. Thostenson, Z. Reng and T.-W. Chou, Advances in the science and technology of carbon nanotubes and their composites: a review, *Compos. Sci. Technol.* **61**, 1899–1912 (2001).
8. Y. Kojima, A. Usuki, M. Kawasaki, A. Okada, Y. Fukushima, T. Kurauchi and O. Kamigaito, Mechanical properties of nylon 6-clay hybrid, *J. Mater. Res.* **8**, 1185–1189 (1993).
9. F. H. Gojny, M. H. G. Wichmann, B. Fiedler and K. Schulte, Influence of different carbon nanotubes on the mechanical properties of epoxy matrix composites — a comparative study, *Compos. Sci. Technol.* **65**, 2300–2313 (2005).
10. K. Wang, L. Chen, J. Wu, M. L. Toh, C. He and A. F. Yee, Epoxy nanocomposites with highly exfoliated clay: mechanical properties and fracture mechanisms, *Macromolecules* **38**, 788–800 (2005).
11. B. W. Rosen, Mechanics of composite strengthening, in: *Fiber Composite Materials*, pp. 37–75. American Society of Metals, Metals Park, Ohio, USA (1965).
12. A. Argon, Fracture of composites, in: *Treatise on Materials Science and Technology*, H. Herman (Ed.), Vol. 1, pp. 79–114. Academic Press, New York, USA (1972).
13. A. K. Subramaniyan and C. T. Sun, Enhancing compressive strength of unidirectional polymeric composites using nanoclay, *Composites Part A* **37**, 2257–2268 (2006).

14. M. Endo, Y. A. Kim, T. Hayashi, Y. Fukai, K. Oshida, M. Terrones, T. Yanagisawa, S. Higaki and M. S. Dresselhaus, Structural characterization of cup-stacked-type nanofibers with an entirely hollow core, *Appl. Phys. Lett.* **80**, 1267–1269 (2002).
15. Y. Iwahori, S. Ishiwata, T. Sumizawa and T. Ishikawa, Mechanical properties improvements in two-phase and three-phase composites using carbon nano-fiber dispersed resin, *Composites Part A* **36**, 1430–1439 (2005).
16. Y.-K. Choi, Y. Gotoh, K. Sugimoto, S. M. Song, T. Yanagisawa and M. Endo, Processing and characterization of epoxy nanocomposites reinforced by cup-stacked carbon nanotubes, *Polymer* **46**, 11489–11498 (2005).
17. T. Yokozeki, Y. Iwahori and S. Ishiwata, Matrix cracking behaviors in carbon fiber/epoxy laminates filled with cup-stacked carbon nanotubes (CSCNTs), *Composites Part A* **38**, 917–924 (2007).
18. T. Yokozeki, Y. Iwahori, S. Ishiwata and K. Enomoto, Mechanical properties of CFRP laminates manufactured from unidirectional prepregs using CSCNT-dispersed epoxy, *Composites Part A* **38**, 2121–2130 (2007).
19. C. T. Sun and J. L. Chen, A simple flow rule for characterizing nonlinear behavior of fiber composites, *J. Compos. Mater.* **23**, 1009–1020 (1989).
20. T. Yokozeki, T. Ogasawara and T. Ishikawa, Effects of fiber nonlinear properties on the compressive strength prediction of unidirectional carbon-fiber composites, *Compos. Sci. Technol.* **65**, 2140–2147 (2005).
21. C. T. Sun and I. Chung, An oblique end-tab design for testing off-axis composite specimens, *Composites* **24**, 619–623 (1993).
22. M. Kawai, M. Morishita, H. Satoh and S. Tomura, Effects of end-tab shape on strain field of unidirectional carbon/epoxy composite specimens subjected to off-axis tension, *Composites Part A* **28**, 267–275 (1997).
23. S. Ogihara, S. Kobayashi and K. L. Reifnider, Characterization of nonlinear behavior of carbon/epoxy unidirectional and angle-ply laminates, *Adv. Compos. Mater.* **11**, 239–254 (2003).
24. B. Budiansky and N. A. Fleck, Compressive failure of fibre composites, *J. Mech. Phys. Solids* **41**, 183–211 (1993).
25. C. R. Schultheisz and A. M. Waas, Compressive failure of composites, part I: testing and micromechanical theories, *Prog. Aerospace Sci.* **32**, 1–42 (1996).
26. P. Berbinau, C. Soutis and I. A. Guz, Compressive failure of 0° unidirectional CFRP laminates by fibre microbuckling, *Compos. Sci. Technol.* **59**, 1451–1455 (1999).